# DISTRIBUTION OF MAGNETIC BIPOLES ON THE SUN OVER THREE SOLAR CYCLES

ANDREY G. TLATOV[1], VALERYA V. VASIL'EVA[1], AND ALEXEI A. PEVTSOV[2]
[1] Kislovodsk Solar Station of Pulkovo Observatory, Russian Federation; tlatov@mail.ru
[2] National Solar Observatory, P.O. Box 62, Sunspot, NM 88349, USA; apevtsov@nso.edu

## ABSTRACT

We employ synoptic full disk longitudinal magnetograms to study latitudinal distribution and orientation (tilt) of magnetic bipoles in the course of sunspot activity during cycles 21, 22, and 23. The data set includes daily observations from the National Solar Observatory at Kitt Peak (1975–2002) and Michelson Doppler Imager on board the *Solar and Heliospheric Observatory* (MDI/*SOHO*, 1996–2009). Bipole pairs were selected on the basis of proximity and flux balance of two neighboring flux elements of opposite polarity. Using the area of the bipoles, we have separated them into small quiet-Sun bipoles (QSBs), ephemeral regions (ERs), and active regions (ARs). We find that in their orientation, ERs and ARs follow Hale–Nicholson polarity rule. As expected, AR tilts follow Joy's law. ERs, however, show significantly larger tilts of opposite sign for a given hemisphere. QSBs are randomly oriented. Unlike ARs, ERs also show a preference in their orientation depending on the polarity of the large-scale magnetic field. These orientation properties may indicate that some ERs may form at or near the photosphere via the random encounter of opposite polarity elements, while others may originate in the convection zone at about the same location as ARs. The combined latitudinal distribution of ERs and ARs exhibits a clear presence of Spörer's butterfly diagram (equatorward drift in the course of a solar cycle). ERs extend the ARs' "wing" of the butterfly diagram to higher latitudes. This high latitude extension of ERs suggests an extended solar cycle with the first magnetic elements of the next cycle developing shortly after the maximum of the previous cycle. The polarity orientation and tilt of ERs may suggest the presence of poloidal fields of two configurations (new cycle and old cycle) in the convection zone at the declining phase of the sunspot cycle.

*Key words:* Sun: activity – Sun: photosphere – Sun: surface magnetism

*Online-only material:* color figures

## 1. INTRODUCTION

The concept of an extended solar cycle introduced by Wilson et al. (1988) is based on observations of solar phenomena spanning the entire solar atmosphere (convection zone, photospheric magnetic bipoles, and corona) and inner heliosphere (for a review, see Harvey 1992). These phenomena include ephemeral regions (ERs)—small (about 20 arcsec in diameter), short-lived (<1 day) bipolar regions with a typical flux of $3 \times 10^{19}$ Mx (see Harvey & Martin 1973; Harvey et al. 1975; Golub et al. 1977). In their orientation, ERs tend to follow the Hale–Nicholson polarity rule albeit with much larger scatter as compared with active regions (ARs). However, at around the peak of the sunspot activity cycle, ERs' orientation in high latitudes (>30°–50°) is opposite to a current sunspot cycle (Wilson et al. 1988; Harvey 1992). As the sunspot cycle progresses, this "cloud" of ERs with reverse orientation (for a current cycle) moves equatorward, eventually joining with Spörer's butterfly diagram of sunspots of the next cycle. In addition to the equatorward arm of ERs, a well observed poleward arm exists in the brightness of the solar corona (e.g., Altrock 1988; Bortzov et al. 1992). The concept has been criticized by Stenflo (1992) who had shown that a butterfly diagram similar in appearance to the extended solar cycle may be described as a simple superposition of eigenmodes in a linear kinetic dynamo model.

In the framework of an extended solar cycle, the appearance of ERs in high latitudes is one of the earliest manifestations of a new solar cycle, and hence, their properties can be used to predict the timing of the next sunspot maximum and its strength using the method outlined in Tlatov & Pevtsov (2010). Such predictive techniques were employed with a different degree of

success by several researchers (e.g., Ol' 1968; Javaraiah 2007; Bhatt et al. 2009).

In previous studies, ERs were identified manually. And although the conclusions about their latitudinal distribution and orientation refer to more than one solar cycle, only limited data sets were used in the identification of ERs. A recent development of automatic procedures for the identification of solar features (see, e.g., Sattarov et al. 2002, for magnetic bipole identification) allows for a complete and more objective investigation of ERs properties and their role in the extended solar cycle. In this investigation, we employ an automatic procedure to select magnetic bipoles and study their orientation in the course of several solar cycles. The rest of this paper is organized as follows. In Section 2, we introduce the data sets and describe our method. Section 3 is devoted to the discussion of the orientation of magnetic bipoles and their latitudinal distribution in the framework of an extended solar cycle, and in Section 4 we discuss our findings.

## 2. DATA AND DATA REDUCTION

### 2.1. Full Disk Magnetogram Data Sets

Three data sets of full disk longitudinal magnetograms were employed in this study: the 512 channel Diode Array Magnetograph (NSO-512) at the National Solar Observatory/Kitt Peak Vacuum Telescope (NSO/KPVT, 1974–1992), the NASA/NSO Spectromagnetograph at NSO/KPVT (SPM, 1992–2002), and the Michelson Doppler Imager on board the *Solar and Heliospheric Observatory* (MDI/*SOHO*, 1996–2009). A detailed description of each instrument can be found elsewhere (e.g., Livingston et al. 1976; Jones et al. 1992; Scherrer et al. 1995).

The NSO-512 data set consists of daily full disk magnetograms from 1974 February 1 to 1992 April 18. The data were taken in the Fe I 8688 Å photospheric spectral line with a pixel size of $1'' \times 1''$ by scanning the solar image with a typical scan duration of about 40 minutes. The SPM data set of the daily full disk magnetogram covers the period from 1992 November 21 to 2003 September 21. The SPM data were taken in several photospheric and chromospheric spectral lines. In this study, we only use observations taken in the Fe I 8688 Å photospheric spectral line with a pixel size of $1''.14 \times 1''.14$. Similar to NSO-512, the data are obtained by scanning the solar image with a typical scan duration of about 1 hr. The MDI data are a synoptic set of full disk magnetograms taken in the Ni I 6768 Å spectral line at a time cadence of 90 minutes (15 magnetograms per day) with a pixel size of about $2'' \times 2''$.

Initial comparison of SPM and NSO-512 magnetograms made at the time of SPM commissioning had shown a reasonably good correlation between the two instruments although some nonlinear effects have been noted (Jones et al. 1992). Later, Wenzler et al. (2006) conducted a detailed comparison between SPM and 512-SM magnetograms and found a nonlinear relation in corresponding magnetic fluxes with a correction coefficient between 1.38 and 1.63. Direct comparison of SPM and MDI magnetograms shows a slight nonlinearity in MDI response to fields stronger than 500 G (Jones & Ceja 2001; Wenzler et al. 2004). Also, MDI flux densities are found to be ~1.3–1.4 times stronger than SPM flux densities.

The mean noise level for NSO-512 (7–8 G; Wenzler et al. 2004; Jones et al. 1992) is slightly higher than for SPM (5 G; Wenzler et al. 2004). The noise level for a 5 minute average MDI magnetogram is about 9 G, and it may have a time-dependent component (Wenzler et al. 2004). Note that the SOI Web site (http://soi.stanford.edu/magnetic/Lev1.8/) cites the per-pixel noise level at about 15 G (30 G) for a 5 minute (1 minute) magnetogram.

In addition, MDI magnetograms can be contaminated by white and black streaks from cosmic rays, which may affect the automatic selection of flux elements. Therefore, the magnetograms strongly affected by cosmic rays were removed from the search for bipoles. However, visual inspection of magnetograms may miss weak cosmic rays, and some magnetograms may still be contaminated. Trails of these weak cosmic rays are usually only about one pixel in width, and their intensity signature can be removed in most cases by simple averaging over neighboring pixels. Such averaging also reduces random noise and improves signal-to-noise ratio. Therefore, MDI magnetograms were averaged over $2 \times 2$ pixels.

### 2.2. Selection of Magnetic Bipoles

To select bipolar pairs, we follow Sattarov et al.'s (2002) bipole identification with an additional criterion of flux balance. First, we identify the flux elements of positive and negative polarity, whose unsigned magnetic flux exceeds a fixed threshold (15 G for NSO-512/SPM and 13 G for MDI), and has a minimum size (area) of 20 millionth of the solar hemisphere (MSH). The flux threshold for MDI magnetograms was selected on the basis that it meets the best agreement with the total number of bipoles identified using SPM data for the same period of time. The size criterion serves as an additional filter for weak-field small-scale features that are more likely to be associated with noisy pixels.

Next, the two families of positive and negative poles were searched for the closest neighbor situated within (2 deg +2× del)
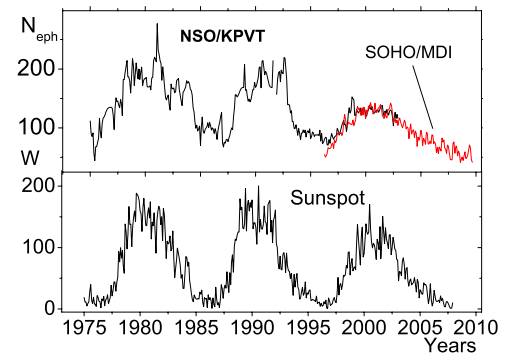


**Figure 1.** Monthly averaged number of magnetic bipoles (upper panel) identified using two NSO magnetographs (NSO-512 and SPM, black solid line) and *SOHO*/MDI data (red solid line). The low panel shows the monthly averaged international sunspot number, *W*.

(A color version of this figure is available in the online journal.)

distance and whose flux matches are within 50%. Here, "deg" stands for one degree in the heliographic coordinate system and "del" is a characteristic size of a feature in degrees. For example, for a circular feature del is its radius. The distance threshold was selected empirically to allow the selection of bipoles of various sizes excluding small-scale (salt-and-pepper) fields.

The search for the next closest neighbor pair begins with an arbitrary pole of positive polarity. If the matching pole of negative polarity is found, a reverse search is performed to find the closest neighbor for the negative pole. If the search returns the same pair of negative and positive poles, the pair is marked and is taken out of the next search. In practice, the routine shows a quick convergence, but it cannot identify multi-pole cases, when, for example, a single positive pole may be connected to more than one pole of negative polarity. Having the 50% flux imbalance threshold helps in selecting bipole pairs even in cases when the true structure may be multi-polar. After initial selection, all pairs that had an area of largest pole smaller than 50 MSH were discarded. This was done to further decrease the influence of noise in bipole selection.

The magnetic field of some features may be structured in a manner that hinders its correct identification. For example, a magnetic flux element that is visually identifiable as part of an AR may be disconnected from the main polarity. Because of its smaller size (area), such a flux element may be classified by our program as non-AR flux (for example, as quiet-Sun flux elements or ephemeral AR). To prevent such misclassification would require a much more sophisticated analysis of the structural relationship between flux elements than we use in our present study. Nevertheless, we believe that our current approach is not significantly affected by these misclassifications. For example, our method requires the presence of two opposite polarity fluxes close to each other. In the above example of a highly structured AR, there would be no opposite polarity flux in close proximity to an AR fragment to form a potential bipolar feature. Therefore, such flux element would be rejected.

Figure 1 shows the monthly averaged total number of bipoles of all sizes identified by our program. There appears to be no significant change in the number of bipoles in 1992, when NSO-512 was replaced by SPM. MDI and SPM bipole numbers also appear to be in good agreement. The total number of bipoles selected in NSO data (NSO-512 and SPM) is about $7 \times 10^5$, which is about 1/3 of the total number of magnetic flux elements (poles) identified during the same period. Thus, about 30% of flux elements were not matched to bipole pairs.
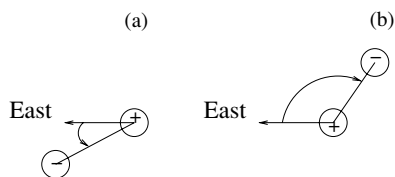
(a)　　　　　　(b)

**Figure 2.** Schematic representation of bipole pairs with (a) negative and (b) positive orientation. The sign of the tilt is defined in respect to the line that originates in the positive polarity pole and points toward solar east. Positive tilt corresponds to an angle in the clockwise direction.

## 3. ORIENTATION OF BIPOLES

After a bipole was identified, we computed its orientation (tilt) as an angle in the clockwise direction between a line pointing from the positive polarity flux element to solar east and a line connecting the positive and negative elements of the bipole. Figure 2 illustrates our definition of tilt.

For the purpose of the following discussion, we have separated all bipoles on four categories based on their total area: smaller than 50 MSH, 100–200 MSH, 200–500 MSH, and larger than 500 MSH. In this nomenclature, the smallest bipoles correspond to quiet-Sun bipoles (QSBs), which have randomly oriented bipolar features; small- to medium-size bipoles are ERs; and the largest bipoles correspond to ARs. Figure 3 provides an example of three types of bipoles identified on a single MDI full disk image.

For each group, we have constructed a histogram of their tilts and computed a preferred tilt for various latitudinal ranges. Figure 4 gives an example of circular histograms for each group of bipoles separately for the northern and southern hemispheres. As expected, bipoles with an area smaller than 50 MSH do not show a preferred orientation. Bipoles with the largest area ($area_{BP} > 500$ MSH) show a strong tilt preference in agreement with the Hale–Nicholson polarity rule and Joy's (tilt) law for ARs. Bipoles in the mid-range of areas do show a slight preference in orientation although their tilts are different from those of AR bipoles. Figure 5 shows average tilt as a function of the area of bipoles ($area_{BP}$). Bipoles with areas smaller than ~300 MSH show significant scatter (about $\pm20°$–$25°$) in their average tilt. Larger bipoles ($area_{BP} \geqslant 500$ MSH) exhibit noticeably smaller scatter in tilts ($\pm10°$). Also, large bipoles follow Joy's law in their average tilt. While bipoles with an $area_{BP} < 300$ MSH have a tilt opposite in sign to Joy's law. The sign of the tilt changes at about $area_{BP} = 300$ MSH. Harvey & Martin (1973) had classified elements with an area of 100–1100 MSH as ERs. If we adopt their definition, Figure 5 suggests that tilt properties of large ERs are similar to ARs, but smaller ERs are tilted opposite to Joy's law (i.e., in bipolar regions the leading polarity has a higher latitude than the following polarity). This opposite tendency in tilt between large ($area_{BP} > 500$ MSH) and small (100 MSH $< area_{BP} < 200$ MSH) bipoles is demonstrated in Figure 6. Note that the latitudinal dependency of the tilt is steeper for small ERs as compared with ARs.

The orientation of bipoles with $area_{BP}$ between 50 and 100 MSH is bi-directional with preference for southeast and northwest orientations for bipoles in the northern hemisphere and northeast and southwest orientations in the southern hemisphere (Figure 7, left column). The distributions become slightly asymmetric when bipoles are separated by the polarity of surrounding large-scale magnetic field (Figure 7, middle and right columns). Here, the polarity of a large-scale field was determined using Hα synoptic maps showing polarity inversion lines from the
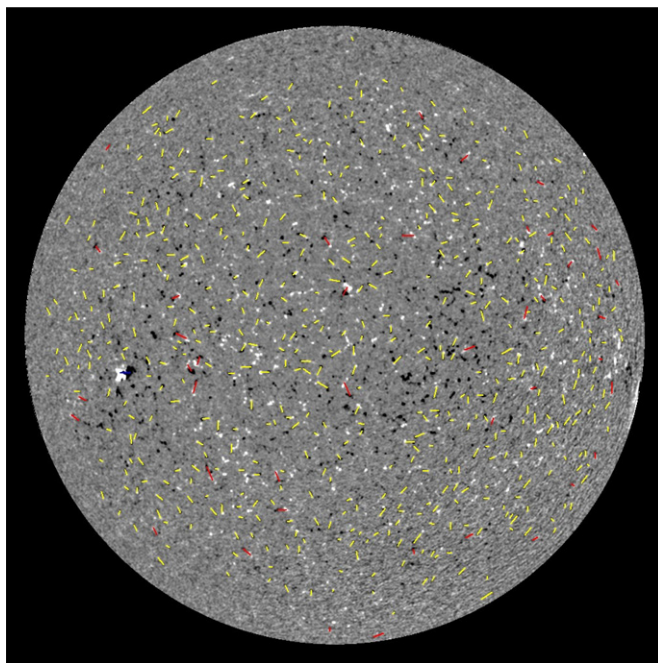


**Figure 3.** Longitudinal MDI magnetogram from 2007 May 8. Three types of bipoles identified by our program are marked by short colored segments: small ARs (blue), ERs (red), and QSBs (yellow).

(A color version of this figure is available in the online journal.)

Kislovodsk High-Altitude Station of the Main (Pulkovo) Astronomical Observatory (http://www.solarstation.ru) and synoptic magnetograms from the Wilcox Solar Observatory. This asymmetry suggests that the connectivity developing between independent poles may be affected by the direction of a large-scale magnetic field. For example, if a positive polarity flux element sits underneath a large-scale field of positive polarity pointing northward, it is more likely to establish a bipolar pair with a negative pole northward from it. Numerical modeling (e.g., DeRosa 2005) has demonstrated the presence of such coupling between small- and large-scale magnetic fields and its effect on the evolution of solar magnetic fields on all spatial scales. Figure 1 in Longcope et al. (2001) shows the possible relation between reconnecting poles later forming an X-ray bright point and a large-scale magnetic field.

Asymmetries in the preferred orientation of bipoles vary with the phase of the solar cycle. Figures 8 and 9 show time–latitude distribution of ERs in the east–west direction. Areas where the number of bipoles with east–west orientation exceeds the number of bipoles with west–east orientation are shown in red. Areas with opposite fractional imbalance are shown in blue. There is a clear difference in an ER's orientation between even and odd solar cycles. The magnetic orientation of ERs in mid-latitudes is similar to ARs. For solar cycle 22, both ERs and ARs have negative (positive) leading polarity field in the northern (southern) hemisphere. This leading polarity pattern is reversed for cycles 21 and 23 in agreement with the Hale–Nicholson polarity rule. However, for ERs the Hale–Nicholson polarity rule is much weaker than for ARs. The preference for a selected polarity orientation does not exceed the 20% level. In other words, the majority of ERs (about 80%) do not show preference for their magnetic orientation. In contrast, only a small fraction of ARs (~10%) disobey the Hale–Nicholson polarity rule.
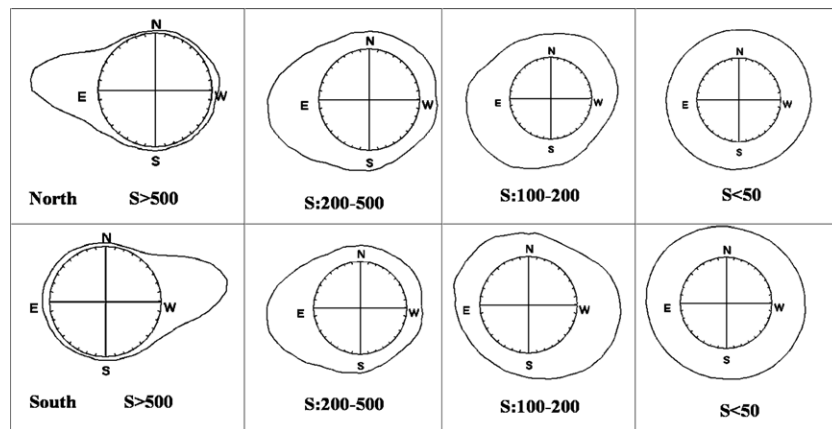
**Figure 4.** Circular histograms of normalized number of bipoles as a function of their tilt for northern (upper row) and southern (lower row) hemispheres for bipoles with areas larger than 500 MSH (left column), 200–500 MSH and 100–200 MSH (two middle columns), and smaller than 50 MSH (right column). The histograms are constructed using bipoles in latitudinal range ±30° identified in *SOHO*/MDI data during 1998–2006.
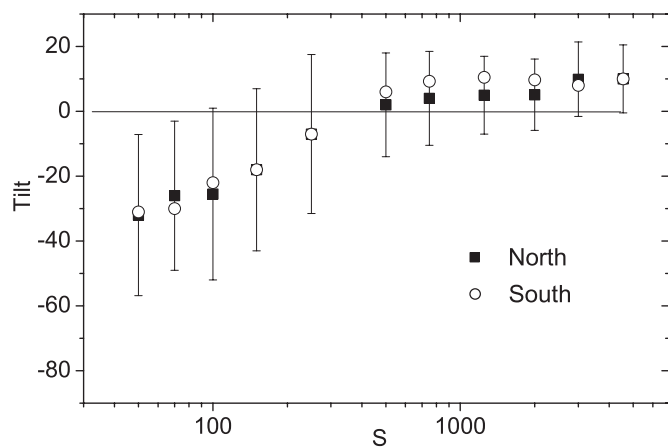


**Figure 5.** Tilt (deg) of bipoles as a function of their area, S in MSH. Filled squares (open circles) show an average tilt for bipoles in northern (southern) hemisphere. Error bars correspond to 1$\sigma$ standard deviation. For display purposes, tilts for the southern hemisphere were multiplied by −1 to allow them to be plotted over the northern hemisphere tilts.



**Figure 6.** Latitudinal variation of average tilt of small ERs (open circles) and ARs (filled squares). In both hemispheres, following polarity in ERs is situated at lower latitude as compared with leading polarity. This orientation is opposite to the ARs' tilt.

One could argue that the orientation of ERs might be defined by (a much stronger) polarity orientation of ARs if ERs were a bi-product of dissipating ARs. Figure 9, however, indicates that the solar cycle of ERs begins much earlier than the AR cycle. The butterfly diagram shows high latitude ERs with a preferential orientation for a given cycle several years prior to the emergence of the first ARs of that cycle. There is also an indication of a polar branch in the ERs' distribution starting at the end of a previous cycle (Figure 9, see contours outlining enhancement in ERs that start about year 1987 at 50° of latitude and drifts poleward). This polar branch might be associated with the poleward arm of enhanced brightness (recently referred to as a "rush to the poles") observed in the solar corona (Altrock 2010).

## 4. DISCUSSION

Figure 9 summarizes tilt properties of ERs in three solar cycles. In their magnetic orientation, ERs follow the Hale–Nicholson polarity rule, but they exhibit inverse latitude–tilt relation as compared with ARs ("inverse" Joy's law). Previous studies of the tilt of ERs arrived at conflicting conclusions. Thus, for example, Harvey-Angel (1993) studied the tilt of ERs in solar cycle 21 and found a weak tendency for
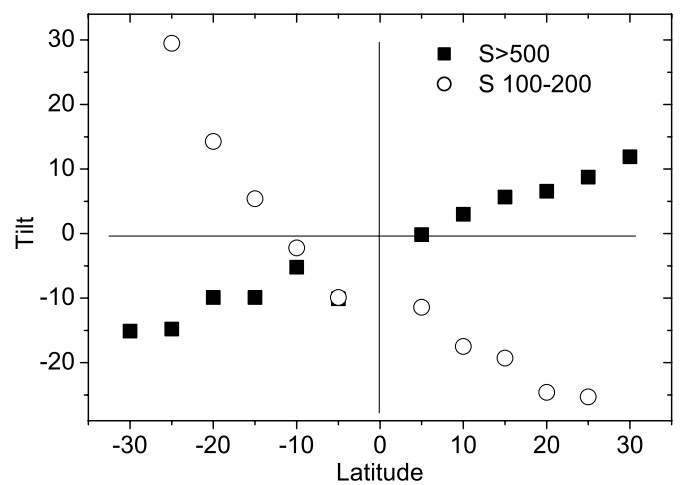
tilts in agreement with Joy's law. On the other hand, Hagenaar et al. (2003) concluded that small ERs do not exhibit a preferred orientation. Our results indicate the presence of a weak preference in orientation of magnetic bipoles associated with ERs. We also found that the smallest bipoles (area$_{BP}$ < 50 MSH) are randomly oriented (Figure 4), which we see as an agreement with Hagenaar et al. (2003). On the other hand, we note that histograms of bipole orientations presented in Figure 9 in Hagenaar et al. (2003) do show the presence of bi-modal distribution in bipole tilts. Our data show such a bi-modal distribution for intermediate size bipoles (Figure 7). A slight dependency in the orientation of bipoles of this size on the orientation of a large-scale magnetic field suggests that these ERs were formed via magnetic reconnection at or near the photosphere.

Traditionally, an AR tilt (Joy's law) is explained by the action of the Coriolis force on a flux tube rising through the convection zone (e.g., Fisher et al. 2000). The amplitude of this tilt depends on how fast the flux tube arises, which in turn is the function of the magnetic flux in the tube. Fan & Fisher (1996) have successfully modeled the process in a framework of a thin flux tube model. The results of their model show good agreement between the observed tilts for flux tubes with strong magnetic flux (typical of ARs). This positive tilt is caused by the action of the Coriolis force upon the diverging flows that develop at
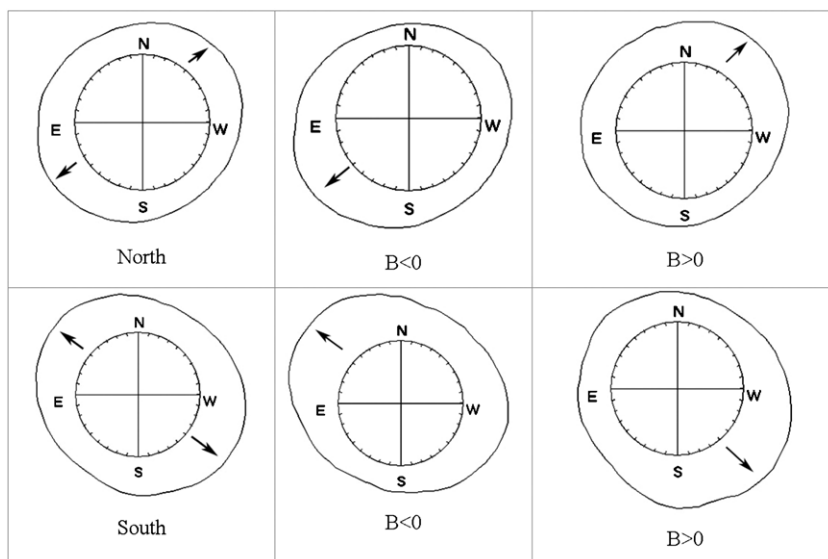
**Figure 7.** Circular histograms of normalized bipole tilt for $50 < \mathrm{area}_{BP} \leqslant 100$ MSH for the northern and southern hemispheres (left column) and separately for bipoles situated in the areas of (middle column) negative and (right column) the positive polarity larger-scale field. Arrows indicate preferential orientation in each distribution. For this plot, we have selected bipoles observed in 1997–2007 and within $\pm 30°$ of latitude.
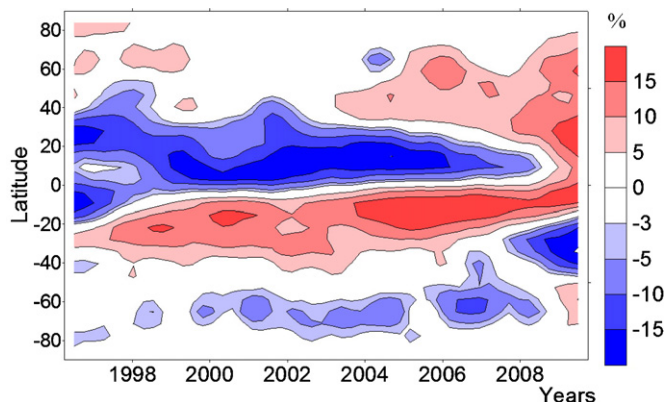


**Figure 8.** Tilt preference in the distribution of bipoles with area $\sim$50–300 MSH as a function of time using *SOHO*/MDI data.
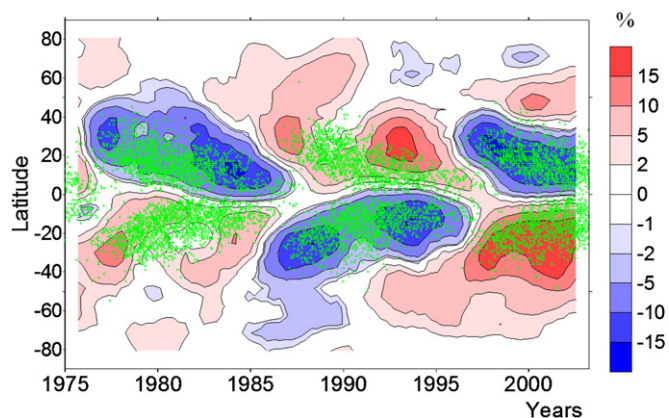


**Figure 9.** Tilt preference in the distribution of bipoles with area $\sim$50–300 MSH as a function of time using NSO data. Green dots show the distribution of ARs.

the apex of the loops with a strong initial field strength. On the other hand, the calculations for weaker fields (typical of ERs) yield tilts of an opposite sense for a given hemisphere. Fan & Fisher (1996) have explained this negative tilt as the action of the Coriolis force on a converging flow at the apex of a magnetic loop rising through the convection zone. The flow starts when the plasma inside the loop is hotter than the external plasma. The model suggests that although this temperature inversion may occur in flux tubes with both strong and weak fields, the effect is stronger (and it starts earlier) for weaker fields thus resulting in the negative tilt. In addition to having an inverse tilt, flux tubes with weaker fields are more susceptible to random distortions of their apex by turbulence in the convection zone. Therefore, they are likely to exhibit a significantly larger dispersion in tilts as compared with ARs. The observed weak preference in orientation of ERs in mid-latitudes (Figures 4 and 6; which is opposite in sign to Joy's law) is in agreement with Fan & Fisher's 1996 modeling. If this interpretation is correct, it indicates that not all ERs are the result of near surface dynamo as suggested by Hagenaar et al. (2003). Some ERs may form at the same location as ARs (i.e., at the base of the convection zone). Steeper latitudinal dependency of tilt for ERs can also be explained by the action of Coriolis force on slowly rising flux tubes. Weaker

flux tubes will spend more time rising through the convection zone, and therefore, the Coriolis force will have a larger effect on them.

Figure 9 suggests that bipoles belonging to a solar cycle number "$n$" appear at high latitudes shortly after the maximum of cycle number "$n-1$." This provides strong support for the idea of an extended solar cycle (e.g., Wilson et al. 1988). Similar early manifestation of cycle 22 (in distribution of small bipoles) was found in cycle 21 by Gillespie et al. (1973). On the basis of these early observations, Harvey-Angel (1993) has suggested that a new solar cycle may begin about 2–3 yr after the polar field reversal, which takes place shortly after the maximum of a current cycle. Our data support these early conclusions. For example, Figure 8 shows the first appearance of ERs with an orientation typical for cycle 24 at around the maximum of cycle 23. Using the average latitude of these high latitude ERs, Tlatov & Pevtsov (2010) had estimated the amplitude of cycle 24 to be at W $= 92 \pm 13$ in units of annual sunspot numbers. However, comparing Figure 8 and 9 for overlapping years, the reader can see that although the distribution of bipoles is very similar between SPM and MDI instruments, there are small differences in high latitudes calling for caution when interpreting some of these features.

Nevertheless, we find that the orientation of ERs and their variation with solar cycle support the idea of an extended solar cycle. The fact that these magnetic bipoles that herald cycle "$n$" have a polarity orientation opposite to the "current" $n-1$ cycle may indicate the presence of large-scale magnetic fields (of a new cycle) at high latitudes at the time of polar field reversal (as was suggested by Tlatov 1996).

## REFERENCES

Altrock, R. C. 1988, in Solar and Stellar Coronal Structure and Dynamics, Proc. 9th Sacramento Peak Summer Symp., ed. R. C. Altrock (Sunspot, NM: National Solar Observatory), 414

Altrock, R. C. 2010, in ASP Conf. Ser., SOHO-23: Understanding a Peculiar Solar Minimum, ed. S. Cranmer, T. Hoeksema, & J. Kohl, in press (arXiv:1002.2401)

Bhatt, N. J., Jain, R., & Aggarwal, M. 2009, Sol. Phys., 260, 225

Bortzov, V. V., Makarov, V. I., & Mikhailutsa, V. P. 1992, Sol. Phys., 137, 395

DeRosa, M. L. 2005, in ASP Conf. Ser. 346, Large-scale Structures and Their Role in Solar Activity, ed. K. Sankarasubramanian, M. Penn, & A. Pevtsov (San Francisco, CA: ASP), 337

Fan, Y., & Fisher, G. H. 1996, Sol. Phys., 166, 17

Fisher, G. H., Fan, Y., Longcope, D. W., Linton, M. G., & Pevtsov, A. A. 2000, Sol. Phys., 192, 119

Gillespie, B., Harvey, J., Livingston, W., & Harvey, K. 1973, ApJ, 186, L85

Golub, L., Krieger, A. S., Harvey, J. W., & Vaiana, G. S. 1977, Sol. Phys., 53, 111

Hagenaar, H. J., Schrijver, C. J., & Title, A. M. 2003, ApJ, 584, 1107

Harvey-Angel, K. L. 1993, PhD thesis, Utrecht Univ.

Harvey, K. L. 1992, in ASP Conf. Proc. 27, The Solar Cycle, ed. K. L. Harvey (San Francisco, CA: ASP), 335

Harvey, K. L., Harvey, J. W., & Martin, S. F. 1975, Sol. Phys., 40, 87

Harvey, K. L., & Martin, S. F. 1973, Sol. Phys., 32, 389

Javaraiah, J. 2007, MNRAS, 377, L34

Jones, H. P., & Ceja, J. A. 2001, in ASP Conf. Proc. 236, Advanced Solar Polarimetry–Theory, Observation, and Instrumentation, ed. M. Sigwarth (San Francisco, CA: ASP), 87

Jones, H. P., Duvall, T. L., Jr., Harvey, J. W., Mahaffey, C. T., Schwitters, J. D., & Simmons, J. E. 1992, Sol. Phys., 139, 211

Livingston, W. C., Harvey, J., Slaughter, C., & Trumbo, D. 1976, Appl. Opt., 15, 40

Longcope, D. W., Kankelborg, C. C., Nelson, J. L., & Pevtsov, A. A. 2001, ApJ, 553, 429

Ol', A. I. 1968, Problems of Arctic and Antarctic, 28, 137 (in Russian)

Sattarov, I., Pevtsov, A. A., Hojaev, A. S., & Sherdonov, C. T. 2002, ApJ, 564, 1042

Scherrer, P. H., et al. 1995, Sol. Phys., 162, 129

Stenflo, J. O. 1992, in ASP Conf. Proc. 27, The Solar Cycle, ed. K. L. Harvey (San Francisco, CA: ASP), 421

Tlatov, A. G. 1996, Radiophys. Quantum Electron., 39, 794

Tlatov, A. G., & Pevtsov, A. A. 2010, Mem. Soc. Astron. Ital., in press

Wenzler, T., Solanki, S. K., Krivova, N. A., & Fluri, D. M. 2004, A&A, 427, 1031

Wenzler, T., Solanki, S. K., Krivova, N. A., & Fröhlich, C. 2006, A&A, 460, 583

Wilson, P. R., Altrock, R. C., Harvey, K. L., Martin, S. F., & Snodgrass, H. B. 1988, Nature, 333, 748